A Study of Earth Radar Returns from Alouette Satellite

by

R. C. Chia
H. H. Doemland
R. K. Moore

CRES Report 37-1

he Remote Sensing Laboratory

April 1967

Supported by
NASA Grant No. NSG-477

CRES
THE UNIVERSITY OF KANSAS • CENTER FOR RESEARCH INC
ENGINEERING SCIENCE DIVISION • LAWRENCE, KANSAS

CRES
CENTER FOR RESEARCH IN ENGINEERING SCIENCE
THE UNIVERSITY OF KANSAS • LAWRENCE • KANSAS

Technical Report
37-1

A STUDY OF EARTH RADAR RETURNS FROM ALOUETTE SATELLITE

by

R. C. Chia
H. H. Doemland
R. K. Moore

April 1967

A STUDY OF EARTH RADAR RETURNS FROM ALOUETTE SATELLITE

Table of Contents

A STUDY OF EARTH RADAR RETURNS FROM ALOUETTE SATELLITE

I. INTRODUCTION

The Alouette satellite I, designated as the 1962 $\beta\alpha$ 1, was constructed by the Defense Research Telecommunications Establishment (DRTE) of the Defense Research Board, Ottawa, Ontario, Canada, and launched on September 29, 1962 into orbit by the U.S. National Aeronautic and Space Administration (NASA). Ionosphere topside sounding was the principal experiment. The Alouette satellite contains, in addition to the sounder, apparatus for counting cosmic ray particles, for observing very low frequency radio waves, and for monitoring engineering performance. The sounder was operated on command from any one of the 13 ground stations around the world. Once started, it functions for 10 minutes, generating 30 transmissions in which the radio frequency changes with time. It then shuts off automatically until commanded on again. Characteristics of the sounder are shown in Table 1 [Chia, et.al., 1965].

All the information collected by the Alouette satellite is telemetered back to ground and recorded onto magnetic tapes.

Since its launch the Alouette operated successfully. Initial studies of the topside sounder ionograms revealed that, in addition to returns from the ionosphere, many ionograms contained good returns from the earth at frequencies above the critical frequency of the ionosphere. These earth returns represented the first radar returns from the earth from satellite altitudes. The Center for Research in Engineering Science of The University of Kansas undertook the study of these earth returns.

Table 1

Alouette Sounder System Parameters

System	Parameter	Remark
T_x	Frequency sweep	0.45 to 11.8 Mc/s in approx. 12 sec.
	Pulse width	100 μ sec.
	Pulse repetition frequency	67 pps.
	Peak pulse power	Approx. 100 W into 400 ohm load.
R_x	Frequency sweep	0.45 to 11.8 Mc/s.
	Noise figure	8 dB.
	Minimum signal detection through antenna matching networks	19 dB above kTB.
Antenna	Dipole 1	150 ft. tip to tip for 0.45 - 4.8 Mc/s.
	Dipole 2	75 ft. tip to tip for 4.8 - 11.8 Mc/s.

Radar observations of the earth from satellite altitudes are potentially valuable as a tool for studying the earth itself, as a technique for evaluating radar observations from the moon and planets and as an aid to the design of radar altimeters for rocket vehicles landing on the earth and planets.

II. THEORY OF EFFECTIVE REFLECTION COEFFICIENT

Radar observations at wavelengths of slightly under a meter have indicated that surfaces smooth to this order are very difficult to find in nature [Edison, et.al., 1960 and Taylor, 1959]. Various theories indicate that a surface is smooth enough to give specular reflection only if the mean square fluctuation about the mean height is less than about a tenth wavelength [Moore, 1957 and Hayre, 1962]. Over the sea, this condition may frequently be met at the wavelength of about 30 m involved in this experiment. It is unlikely that land surfaces will be this smooth over a distance as great as that indicated by the diameter (347 km) of the illuminated circle directly beneath the satellite. Consequently, it is to be expected that land echoes will be primarily due to scattering rather than Fresnel reflection, and also sea echoes may often be scattered.

The power received from a rough scattering surface is expressed by

$$W_r = \int_{\substack{\text{Illuminated} \\ \text{Area}}} \frac{W_t \lambda^2 G^2}{(4\pi)^3 R^4} \sigma_o \, dA \qquad (1)$$

where W_t = Transmitted power

G = Antenna gain

R = Distance from the transmitter to a point in the illuminated area

σ_o = Scattering cross section per unit area

A = Illuminated area

λ = Wavelength.

For pulse-length limitation of the illuminated area on the ground with rectangular pulses and essentially constant antenna gain, this integral reduces for the "altitude signal" to

$$W_r = \frac{W_t \lambda^2 G^2}{2(4\pi)^2} \int_h^{h + \frac{c\tau}{2}} \frac{\sigma_o dR}{R^3} \qquad (2)$$

where h = Altitude

c = Velocity of light

τ = Pulse length.

We may express this integral in terms of the angle rather than the range in which case it is

$$W_r = \frac{W_t \lambda^2 G^2}{2(4\pi)^2 h^2} \int_o^{\tan^{-1} \frac{c\tau}{h}} \sigma_o(\Theta) \sin\Theta \cos\Theta d\Theta \qquad (3)$$

where Θ is the angle made by an element on the ground with the vertical.

Experiment and theory both indicate that for surfaces that are relatively smooth with respect to a wavelength, σ_o decreases rapidly with increasing Θ in the vicinity of the vertical. It is likely that most grounds (at least outside of mountain areas) will satisfy this criterion for 30 m wavelength. Consequently, most of the contribution to the integral normally comes from angles considerably under 10 deg. This means

$$\sigma_o\left(\tan^{-1}\sqrt{\frac{c\tau}{h}}\right) << \sigma_o(0). \tag{4}$$

When this situation prevails, the upper limit determined by pulse length is immaterial. That is, the radiation is essentially limited by the beam angle of the backscattering rather than by the pulse length. When this is true an arbitrary upper limit such as $\frac{\pi}{2}$ may be placed on the integral without significant error:

$$W_r \approx \frac{W_t \lambda^2 G^2}{(4\pi)^2 (2h)^2} \int_o^{\frac{\pi}{2}} \sigma_o(\Theta) \sin 2\Theta d\Theta \ . \tag{5}$$

This equation is the same as that for a specular reflection where the integral is the square of the Fresnel reflection coefficient. Thus, we may define

$$K_{eff}^2 = \int_o^{\frac{\pi}{2}} \sigma_o(\Theta) \sin 2\Theta d\Theta \tag{6}$$

as the square of the effective Fresnel reflection coefficient, K_{eff}.

Beam-width-limited illumination is characterized by the expression

$$W_r = \left[\frac{W_t \lambda^2 G^2}{(4\pi)^2 (2h)^2}\right] \int_o^{\Theta_o} \sigma_o(\Theta) \sin 2\Theta d\Theta \tag{7}$$

where Θ_o is the limit of the beam, in which the variation with height is the same as that for a specular reflection. Pulse-length limitation, on the other hand, corresponds to a different variation with height [Moore et.al., 1957].

Thus, use of this effective reflection coefficient implies beam-width limitations. In this case, the beam is set by the scattering coefficient rather than by the width of the antenna pattern as it is in some microwave vertical-looking radars.

The use of the effective reflection coefficient may or may not imply that Fresnel reflection does, in fact, occur. If Fresnel reflection occurs, the signal should not fade in amplitude. If scattering occurs, the signal should fade, as contributions from the different scatterers add successively in and out of phase.

III. DATA ANALYSIS

The upper frequency limit of the sounder is lower than one would prefer for ground echo studies. Because of a large number of interferring signals in the top 2 mc of the sweep range, it was decided to concentrate on the frequency range from 8.5 to 9.5 Mc/s for ground echo studied.

Figure 1 shows a simplified block diagram of the sounder. Computation of system sensitivity can be understood better by referring to this diagram. Unfortunately the calibrations had to be obtained on the ground somewhat piecemeal because the antennae were not self-supporting in the presence of gravity. Calibration curves obtained before launch were supplied by DRTE for:

1) Radiated power
2) Transmitter output
3) Mismatch loss
4) AGC vs. frequency
5) AGC variation with supply voltage
6) AGC vs. input.

These curves may be found in the Appendix.

Based on these calibration curves, it was possible to calculate [Chia, et. al., 1965] the power received at the antenna for a given receiver output.

Figure 1.

SIMPLIFIED BLOCK DIAGRAM OF THE SOUNDER

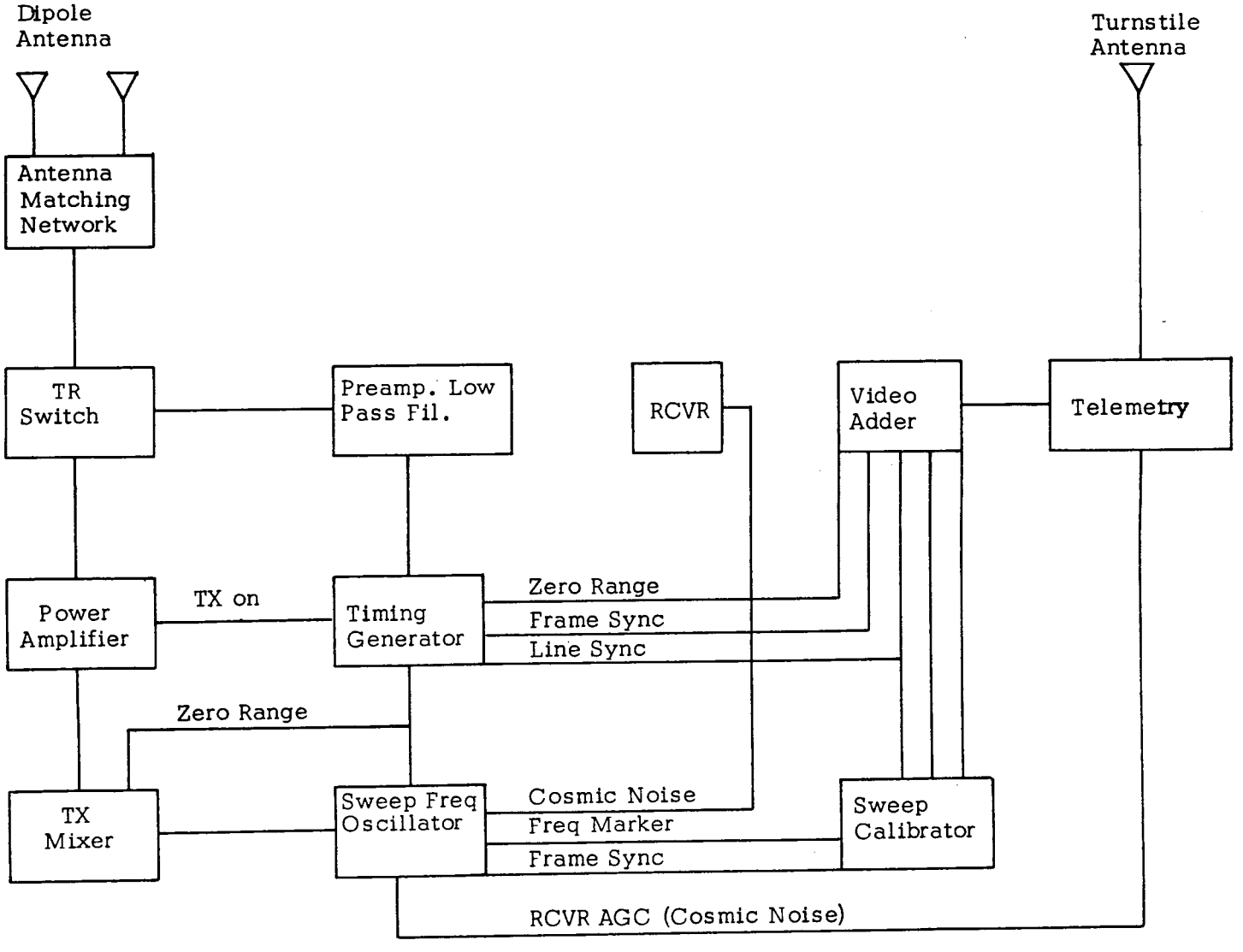

The video signal contains the reference line sync, the zero time reference, and the echo returns. The height of the returned echo is measured in terms of percentage of the line sync unit. Then using AGC information the echo height is converted to microvolts at the receiver input.

The sounder receiver AGC is controlled by the level of externally impressed noise. At each imposed frequency marker, AGC returns to zero volts. Thus the magnitude of the AGC can be decoded by measuring the deviation from the reference level and comparing it with the calibrated value. The calibrated chart reveals the input magnitude through the AGC and the echo height readings.

The time code can be used to check on the satellite map, the ephemeris, prepared by NASA, so that the actual target area can be correctly located.

Signal tapes for a total of 53 passes of the satellite were obtained from DRTE in two different groups. The first group of 31 tapes was received in October, 1963. It contains 31 passes mainly over the Southern hemisphere. The second group of 11 tapes was received in June, 1965. Most of its 22 passes are over the Northern hemisphere.

In many locations the ground signal is too weak to be measured accurately. This is due in part to the scattering properties of the ground, in part to the ionosphere, and in large part to the presence of many interfering signals at various frequencies within the range of interest. Interfering signals are particularly bad in the Northern hemisphere. The best ground echoes so far obtained are those reflected from the continent of Australia. Ground returns from Northern hemisphere often contain only a few pulses in the appropriate range. After analysis of the data, 70 points were used for the final studies.

Variations in the performance of the telemetry link do not affect the result because a "line sync unit" is the standard amplitude measure. This is determined by a calibration pulse (transmitted once for each transmitter pulse) which accurately determines the transfer gain for the telemetry recording and playing-back system.

Table 2 illustrates the anticipated errors in the various quantities for both ionosphere and ground echoes. Maximum overall RMS error has been obtained for these. It is $\pm$ 3.35 dB.

Table 2

Summary of Errors

Parameter	Variation Range	Selected Reference	Max. error in dB
Signal reading	± 4 percent		
Line Sync reading	± 3 percent		
AGC reading	± 1 percent		
AGC input curves			± 1.50
Reading errors			± 1.50
Antenna gain		1.31	± 1.50
For lower frequency:			
Frequency	4.9-5.5 Mc/s	5.2 Mc/s	± 0.25
Transmitted power	7-9 dB below 100W	7 dB below 100W	± 1.20
Altitude	600-800 km	700 km	± 1.00
RCVR input Z_R		366-j99 ohm	± 1.00
Mismatch loss		2.86 dB	± 1.00
For higher frequency:			
Frequency	8.7-9.3 Mc/s	9.0 Mc/s	± 0.15
Transmitted power	6.6-8.2 dB below 100W	7 dB below 100W	± 1.20
Altitude	1004-1050 km	1000 km	- 0.20
RCVR input Z_R		311-j66 ohm	± 1.00
Mismatch loss		1.7 dB	± 0.50
Maximum possible overall RMS error			± 3.35

IV. EXPERIMENTAL RESULTS

Table 3 shows the effective reflection coefficients calculated for the selected terrains on both the absolute and relative basis. The descriptions of the targets were obtained from examination of detailed vegetation maps of the areas involved. The states of the sea were not known exactly at the sampled time. Only the wind speed could be obtained from the nearby weather stations. It was insufficient to correlate the echo strength with the sea states at the particular instants.

Table 3

Local Time		Location			Terrain	Reflection Coefficient (calculated in dB)			Remark
						A	B	C	
Date	Hr&Min.	Long.	Lat.			Iono. K_i^2	Ground K_g^2	$(K_g/K_i)^2$	
Oct. 27 '62	05 55	37.8° W	55.3° S	South Atlantic	Ocean	-1.44	-6.95	-5.51	Tape 46A
	06 17	33.6° W	42.2° S			-0.30	-4.70	-4.40	
	06 18	33.3° W	41.1° S			-0.30	-3.58	-3.28	
	06 22	32.5° W	37.1° S			-1.15	-5.29	-4.14	
Oct. 27 '62	06 00	63.3° W	52.8° S	South Atlantic	Ocean	0.07	-2.68	-2.75	Tape 46B
	06 02	63.4° W	51.6° S			-0.58	-2.72	-2.14	
	06 11	61.0° W	45.9° S			-0.14	-2.98	-2.84	
Oct. 27 '62	20 16	29.7° W	66.3° S	South Atlantic	Ocean		-5.72		Tape 47A
Oct. 28 '62	05 40	77.1° W	58.0° S	South Atlantic	Ocean	-0.96	-6.64	-5.68	Tape 48B
Oct. 28 '62	06 02	46.1° W	46.8° S	South Atlantic	Ocean	0.16	-3.14	-3.30	Tape 48A
	06 04	45.9° W	45.7° S			-4.36	-8.90	-4.54	
Oct. 28 '62	19 15	52.6° W	42.8° S	South Atlantic	Ocean	-4.84	-9.18	-4.34	Tape 49
	19 32	49.1° W	53.9° S			0.25	-5.85	-6.10	
Nov. 17 '62	16 44	66.4° W	47.8° S	South Atlantic	Ocean near coast line (Argentina)	-1.98	-3.65	-1.67	Tape 70B
	16 46	66.0° W	48.7° S			-0.89	-4.56	-3.67	
	16 49	65.4° W	50.7° S			-0.74	-3.26	-2.52	

(continued next page)

Table 3 (continued)

Local Time		Location			Terrain	Reflection Coefficient (calculated in dB)			Remark
Date	Hr.&Min.	Long.	Lat.			A Iono. K_i^2	B Ground K_g^2	C $(K_g/K_i)^2$	
Jan. 22 '63	07 41	133.2° E	16.3° S	AUSTRALIA	Low Arid Woodland	-1.53	-6.86	-5.33	Tape 62
	07 43	133.3° E	17.2° S		Semi Arid Tuss. Grsld	-0.45	-9.04	-8.59	
	07 44	133.6° E	20.1° S		Semi Arid Shrub	-0.25	-7.15	-6.90	
	07 47	134.1° E	24.0° S		Semi Arid Savannah	-0.01	-4.11	-4.10	
	07 49	134.4° E	26.0° S		Low Arid Woodland	-0.19	-7.65	-7.46	
	07 50	134.5° E	27.0° S		Semi Arid Tuss. Grsld	0.08	-8.39	-8.47	
	07 51	134.8° E	29.0° S		Arid Scrub	0.02	-7.72	-7.74	
Jan. 27 '63	18 16	130.5° E	39.2° S		Sea (G. A. Bight)	-3.14	-9.40	-6.26	Tape 64A
	18 17	130.7° E	38.1° S		"	-0.93	-5.99	-5.06	
	18 24	131.9° E	31.4° S		Semi Arid Mallee	-3.11	-8.97	-5.86	
	18 25	132.1° E	30.3° S		Arid Scrub	-3.85	-9.11	-5.26	
Jan. 28 '63	07 05	146.3° E	30.2° S		Temp. Tree Savannah	0.05	-6.93	-6.98	Tape 64B
	07 06	146.5° E	31.2° S		Temp. Woodland	-1.72	-5.92	-4.20	
	07 14	147.9° E	39.2° S		Ocean	-2.87	-7.50	-4.63	
	07 19	148.8° E	43.1° S		"	-1.76	-5.82	-4.06	
Jan. 28 '63	18 02	144.6° E	44.0° S		Ocean	1.35	-4.90	-6.25	Tape 65A
	18 07	145.4° E	40.1° S		Sea (Bass Str.)	-1.86	-9.44	-7.58	
	18 16	147.1° E	31.0° S		Temp. Tree Savannah	-2.84	-8.64	-5.80	
	18 17	147.2° E	30.0° S		"	-0.24	-6.42	-6.18	
	18 19	147.5° E	28.1° S		Arid Scrub + Trop. Wd.	-0.50	-4.24	-3.74	
	18 22	148.1° E	24.0° S		Layered Scrub	-0.90	-7.45	-6.55	

(continued next page)

Table 3 (continued)

Local Time		Location			Terrain	Reflection Coefficient (calculated in dB)			Remark
Date	Hr.&Min.	Long.	Lat.			A Iono. K_i^2	B Ground K_g^2	C $(K_g/K_i)^2$	
Jan. 29 '63	05 08	136.9° E	40.5° S	South Pacific	Ocean	-2.39	-6.97	-4.58	Tape 65B
Mar. 16 '63	13 16	97.7° W	53.1° N	Canada	Lake Winnipeg	-1.32	-6.68	-5.36	Tape 6
	13 34	93.8° W	60.7° N		Hudson Bay	-0.66	-5.35	-4.69	
Mar. 18 '63	13 16	90.5° W	59.9° N				-8.24		
	13 27	88.0° W	63.6° N				-6.88		
Nov. 9 '63	06 39	84.6° W	65.6° N	Canada	Foxe Basin (ice covered)		-6.68		Tape 1
	06 55	80.8° W	68.3° N				-4.76		
	07 05	78.4° W	70.1° N				-6.30		
Nov. 13 '63	16 21	114.7° W	25.6° N	Eastern Pacific	Ocean near coast line of Mexico	-0.62	-9.00	-8.38	Tape 2
	16 23	114.3° W	22.6° N			-1.01	-5.02	-4.01	
Nov. 15 '63	16 08	110.6° W	22.7° N			-2.05	-2.72	-0.67	
Nov. 22 '63	14 31	171.1° W	56.0° N	North Pacific	Ocean	-0.08	-3.46	-3.38	Tape 10
	14 35	170.4° W	54.1° N			-0.09	-6.52	-6.44	
	14 37	170.0° W	53.1° N			0.02	-5.06	-5.08	
	14 38	169.6° W	52.1° N			0.16	-5.59	-5.75	
	14 40	169.3° W	51.2° N			-0.90	-6.66	-5.76	
	14 42	169.0° W	50.2° N			-0.44	-5.53	-5.09	
	14 45	168.4° W	48.2° N			0.04	-3.86	-3.90	
	14 48	167.8° W	46.3° N			-0.97	-3.99	-3.02	

(continued next page)

Table 3 (continued)

Local Time		Location			Terrain	Reflection Coefficient (calculated in dB)			Remark
						A	B	C	
Date	Hr.&Min.	Long.	Lat.			Iono. K_i^2	Ground K_g^2	$(K_g/K_i)^2$	
Nov. 23 '63	14 28	155.1° W	53.6° N	North Pacific	Ocean	0.07	-3.62	-3.69	Tape 10 (cont'd)
	14 37	153.3° W	48.8° N			0.03	-4.65	-4.68	
	14 38	153.0° W	47.7° N			-1.16	-3.90	-2.74	
	14 40	152.7° W	46.8° N			-0.76	-3.47	-2.71	
	14 41	152.5° W	45.8° N			-0.50	-3.54	-3.04	
Nov. 27 '63	14 29	114.9° W	28.0° N	Eastern Pacific	Ocean near coast line of Mexico	-2.08	-3.62	-1.54	Tape 3
	14 32	114.4° W	25.0° N			-0.03	-6.72	-6.69	
	14 33	114.3° W	24.0° N			-0.37	-7.72	-7.35	
	14 34	114.2° W	23.0° N			-3.70	-6.09	-2.39	
Dec. 18 '63	11 46	114.5° W	27.2° N	Eastern Pacific	Ocean near coast line of Mexico	-2.58	-6.58	-4.00	Tape 4
	11 47	114.4° W	26.2° N			-2.12	-5.62	-3.50	
	11 49	114.0° W	23.3° N			-2.67	-4.98	-2.31	
Dec. 22 '63	11 04	109.0° W	32.5° N	USA (Ariz, NM)	Needle leaved forest	-2.80	-6.50	-3.70	
	11 06	108.6° W	29.4° N	Mexico		-2.28	-2.82	-0.54	

Attenuation in the ionosphere at 9 Mc/s has been studied. It was found that an accurate instant correction would be too much involved. A rough correction by the Quiet Day curve method [Mitra and Shain, 1953; Steiger and Warwick, 1961] was attempted for correction factors ranging from 0.65 to 6.5 dB.

Table 4 compares the results of the power reflection coefficients with comparable data from other observers at other frequencies.

Table 4

Power Reflection Coefficients at Several Different Frequencies

Observer	Frequency	Altitude	Terrain			
			Forest	Desert	Sand	Water
Sandia[c] Corp.	415 Mc/s	12,000 ft.	-12 to -21 dB	-13 dB		-1[b] dB
		8,000 ft.			-6 dB	
		7,000 ft.				+1[a] dB
	3800 Mc/s	12,000 ft.	-13 to -16 dB	-14 dB		+2[b] dB
		7,000 ft.				+1[a] dB
Auburn[d] University	1600 Mc/s	2,000 to 70,000 ft.				-3[a] to -5[b] dB
Alouette	9 Mc/s	1000 km	-7 to -14 dB	-3.5 to -10 dB		-6 to 0 dB

[a]Smooth water.
[b]Rough water.
[c]Edison et. al., 1960.
[d]Summer, 1963.

A. K_g/K_i Correction

As stated above, the effective reflection coefficient, K_i, of the ionosphere was calculated using data at approximately 5 MHz. The effective reflection coefficient of the ground, K_g, was calculated from data at 8.5 to 9.5 MHz. These figures are given in columns A and B respectively of Table 3. Column C represents a "corrected" K_g. The ratio of K_g/K_i in dB is

$$20 \log \frac{K_g(\text{absolute})}{K_i(\text{absolute})} = 20 \log K_g(\text{abs}) - 20 \log K_i(\text{abs}) \quad .$$

If $K_i(\text{abs}) < 1$ then this ratio in dB is the effective reflection coefficient of the ground, K_g, that would result if there had been no ionosphere present. This correction suffers from the fact that K_i is at 5 MHz and K_g is at 8.5 to 9.5 MHz. However, this is the best that can be done for this type of correction.

B. Attenuation of R.F. in Ionosphere by Collision Frequency

Attenuation a wave suffers in the ionosphere due to electrons colliding with heavy particles has been discussed by many papers. One of the theoretical expressions for the absorption coefficient K given by Ratcliffe [19] has the form

$$K = \frac{1}{2c\mu} \cdot \frac{\omega_N^2 \nu}{(\omega \pm \omega_L)^2 + \nu^2} \quad \text{nepers/m} \quad .$$

where c = the velocity of light in free space

μ = the real part of the refraction index

ν = the average frequency of collision between electron and heavy particles

ω = the wave signal frequency

ω_L = the longitudinal gyro-frequency

ω_N = the ionosphere plasma frequency

This equation is derived by introducing into the basic equation of motion of a single electron a "viscous damping force" - $m\nu\dot{r}$ with m being the mass and $\dot{r}$ the velocity of the electron. It is applicable to quasi-longitudinal propagation. In this equation, we can see that only c and ω are independent of position. Other parameters vary from point to point along a vertical path of interest at a particular time; thus, if the instantaneous attenuation is to be found, the correct values for these parameters must be found first.

Besides finding the magnitude of the collision frequency ν and its relation with ω_N or ω_H (see Appendix), we need furthermore to know the condition of the bottom side of the ionosphere in addition to the simultaneously measured ionospheric conditions. Detailed studies of the instantaneous absorption require details which are difficult to obtain for the locations of the Alouette.

C. The Quiet Day Curve and Its Use

Since the instantaneous absorption could not be found, we turned to another method, using the quiet day curve to try to find a reasonable average approximate correction factor.

The idea of the quiet day curve [Mitra and Shain, 1953; Steiger and Warwick, 1961] is basically as follows:

Every kind of radio wave which travels through the ionosphere is attenuated, as is cosmic radio noise at the frequency of interest. It was assumed that the minimum ionosphere attenuation occurs between 0100 and 0600 hours local time. These cosmic-noise levels were plotted against the corresponding sidereal time for an entire solar year, or a complete sidereal day. The envelope, referred as the quiet day curve, is drawn through the maximum of the scatter distribution. It is assumed to represent incoming signals that have not suffered any attenuation.

Fortunately for our purpose, a 9 mc antenna was constructed by the High Altitude Observatory, University of Colorado, near Boulder, Colorado. A set of recorded cosmic noise for nine months of 1964 was reduced at CRES and the quiet day curve determined (as shown in figure 2).

Figure 2.

QUIET DAY CURVE
9 mc., Boulder, Colorado

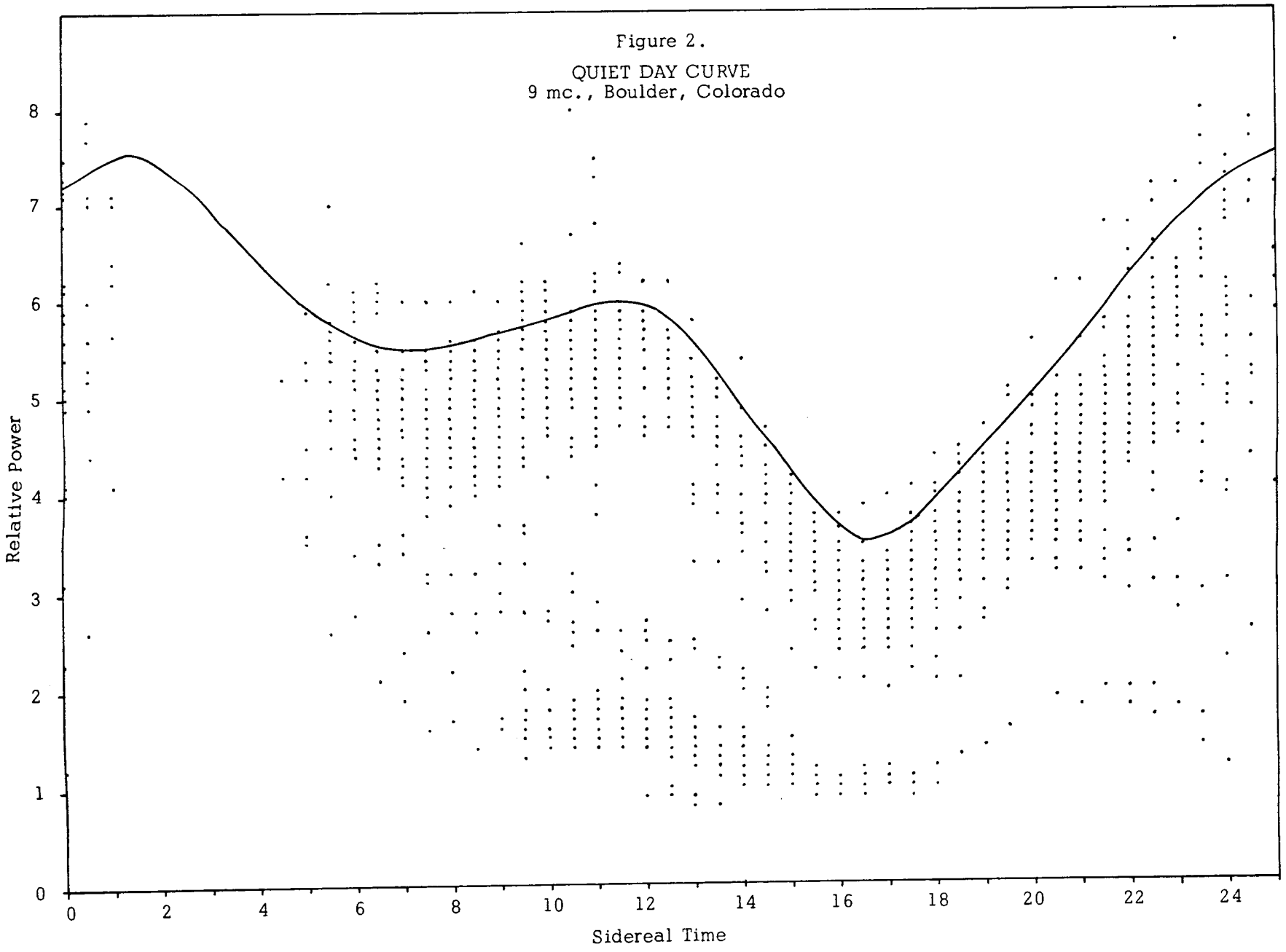

In order to apply the idea of the quiet day curve to the correction of the Alouette satellite data, several assumptions were made, namely:

1) the ionosphere is symmetrical about the earth's geomagnetic axis, so that the first order correction can thus be made in both hemispheres from observations in the northern hemisphere;

2) the quiet day curve is invariant with time, so that the curve reduced from the 1964 period can be used for any other time;

3) the same correction factor may be applied to $\pm$ 10° on each side of the geomagnetic latitude over Boulder, Colorado (135° W 40° N geographic location) and over the same region in the southern hemisphere;

4) the correction factor is taken as the ratio of the quiet day curve reading to the attenuated record at the sideral time of interest.

The correction factors thus obtained under these assumptions range from 0.65 dB to 6.5 dB and were applied to selected points in column B of Table 3.

The reduced points which do not fall within the regions stated in condition (3) have not been corrected. The corrected effective reflection coefficients are listed in column B of Table 5.

D. Average Diurnal Attenuation

Using the 9 MHz cosmic radio noise data mentioned in section B above, curves for the average diurnal attenuation of the ionosphere vs. Mountain Standard Time were plotted. These curves are shown in figures 3 and 4. Figure 3 is for the summer and figure 4 for the winter. Local time for the satellite pass was used to obtain the correction. These corrections varied between .5 dB and 3.4 dB. The results are shown in column C of Table 5.

Figure 3.

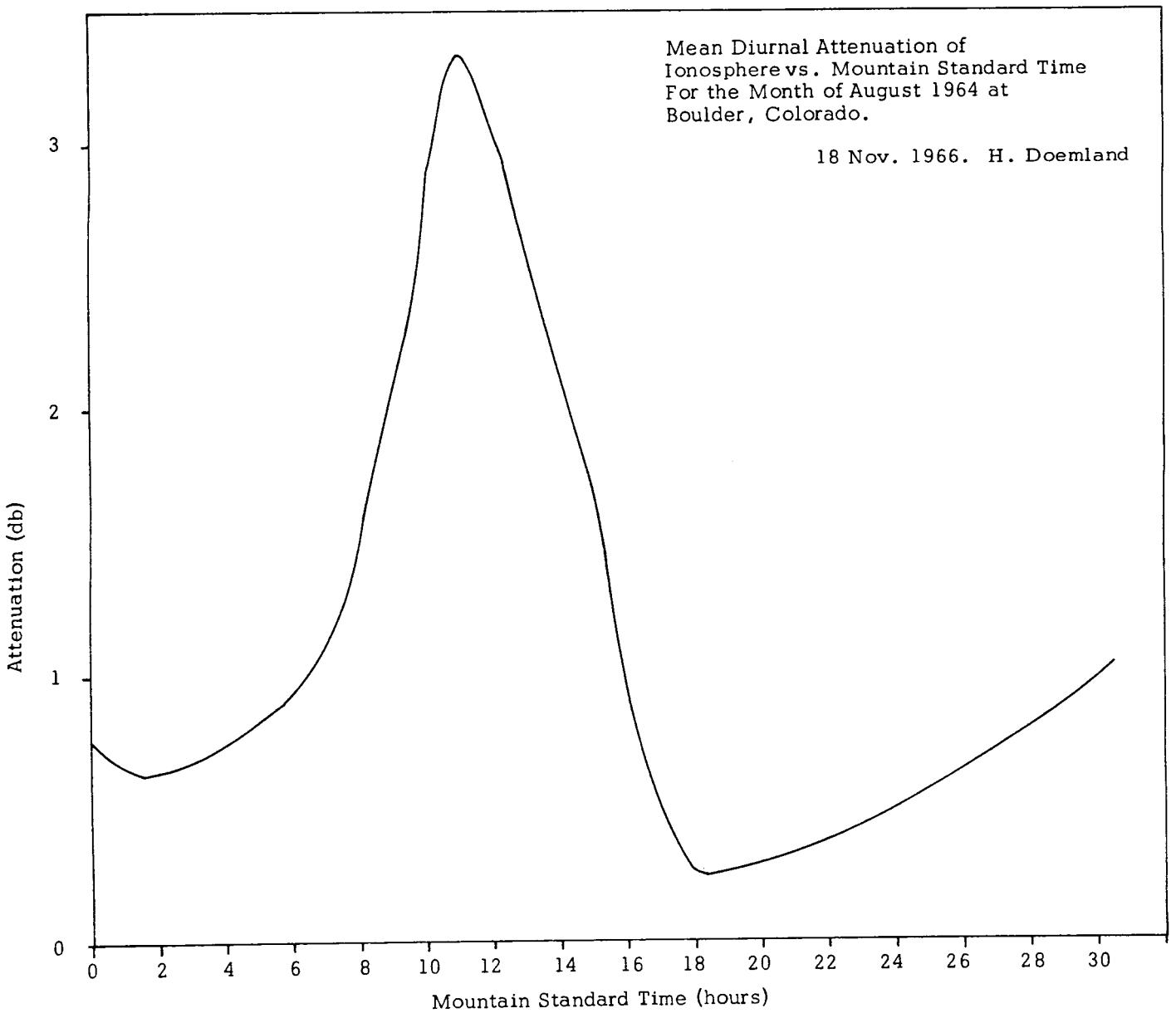
Mean Diurnal Attenuation of
Ionosphere vs. Mountain Standard Time
For the Month of August 1964 at
Boulder, Colorado.
18 Nov. 1966. H. Doemland
Attenuation (db)
0
1
2
3
0
2
4
6
8
10
12
14
16
18
20
22
24
26
28
30
Mountain Standard Time (hours)

Figure 4.

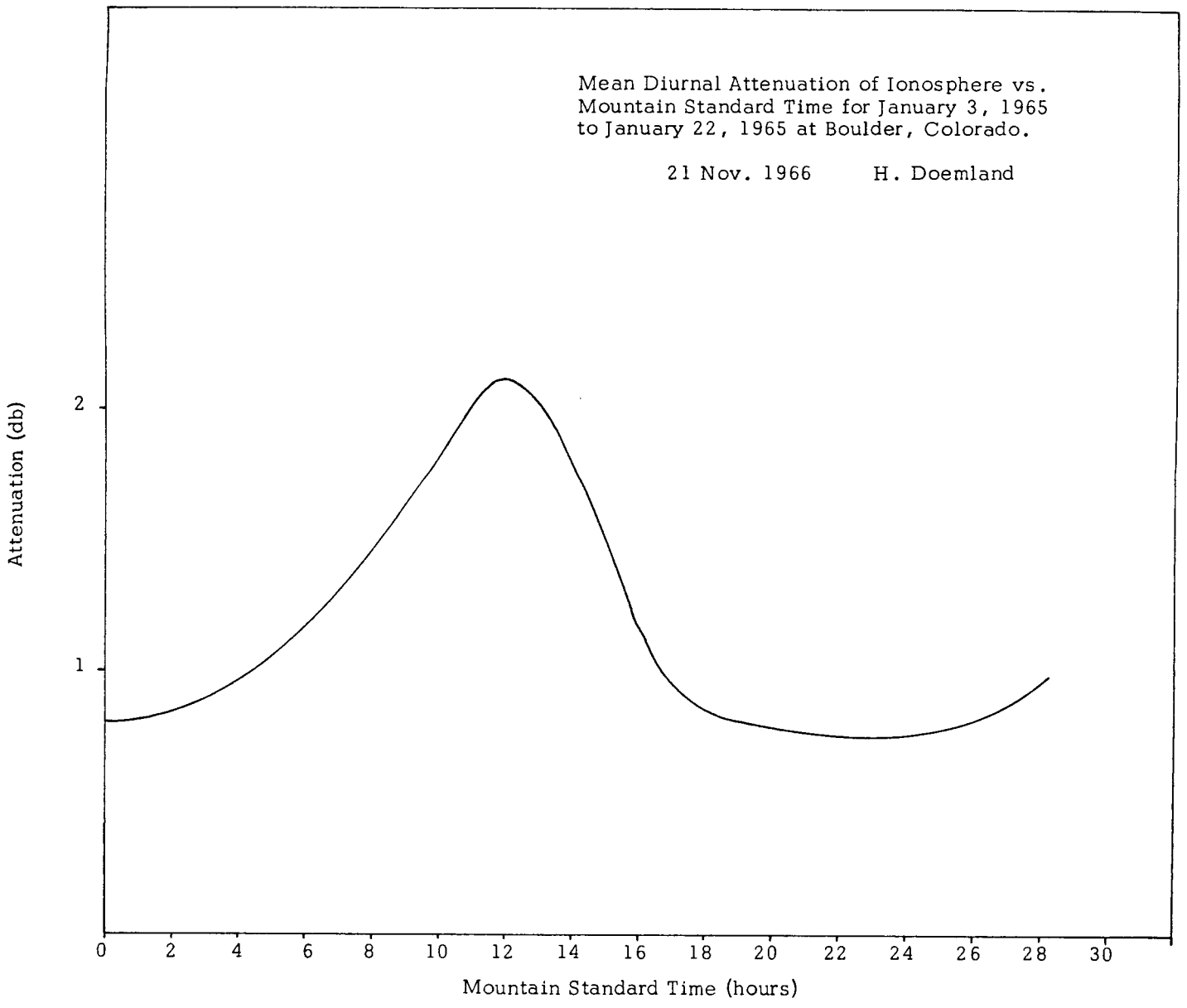
Mean Diurnal Attenuation of Ionosphere vs.
Mountain Standard Time for January 3, 1965
to January 22, 1965 at Boulder, Colorado.
21 Nov. 1966 H. Doemland
Attenuation (db)
2
1
0 2 4 6 8 10 12 14 16 18 20 22 24 26 28 30
Mountain Standard Time (hours)

Table 5

Line	Local Time		Sidereal Time	Geographic Location	Remarks	Reflection Coefficient							Averages of Column C		Range of K_g^2 for RMS error of ± 3.35 dB	
						K_1^2 (dB)	Uncorrected K_g^2 (dB)	Quiet Day Curve Correction dB	Mean Diurnal Attenuation Correction dB	A. $(K_g/K_1)^2$ (dB)	B. Quiet Day Correction K_g^2 (dB)	C. Mean Diurnal Attenuation Correction K_g^2 (dB)	K_g^2 absolute	K_g^2 (dB)	absolute	dB
1	Oct. 27, 1962	0555	08-15-37	37.8°W, 55.3°S	South Atlantic Ocean	-1.44	- 6.95	6.04	1.6	- 5.51	- .91	- 5.35				
2		0600	08-17-54	63.3°W, 52.8°S	"	0.07	- 2.68	6.45	1.6	- 2.75	+ 3.77	- 1.08				
3		0602	08-20-04	63.4°W, 51.6°S	"	- .58	- 2.72	6.45	1.6	- 2.14	+ 3.73	- 1.12	.438	- 3.59	.202 to .578	- 6.94 to -2.38
4	Oct. 28, 1962	0540	08-04-32	77.1°W, 58.0°S	"	- .96	- 6.64	6.37	1.6	- 5.68	- .27	- 5.04				
5		1932	21-58-24	49.1°W, 53.9°S	"	.25	- 5.85	4.91	.5	- 6.10	- .94	- 5.35				
6	Jan. 27, 1963	1816	02-40-35	130.5°E, 39.2°S	Australian Continent	-3.14	- 9.40	1.11	1.4	- 6.26	- 8.29	- 8.00				
7		1817	02-41-43	130.7°E, 38.1°S	"	- .93	- 5.99	1.11	1.4	- 5.06	- 4.88	- 4.59	0.201	-6.97	.093 to .434	-10.32 to -3.62
8		1824	02-48-46	131.9°E, 31.4°S	"	-3.11	- 8.97	1.43	1.4	- 5.86	- 7.54	- 7.57				
9		1825	02-49-43	132.1°E, 30.3°S	"	-3.85	- 9.11	1.43	1.4	- 5.26	- 7.68	- 7.71				
10	Jan. 28, 1963	1802	02-31-00	144.6°E, 44.0°S	South Pacific Ocean	1.35	- 4.90	1.58	1.4	- 6.25	- 3.32	- 3.50				
11		1807	02-35-48	145.4°E, 40.1°S	"	-1.86	- 9.44	1.58	1.4	- 7.58	- 7.86	- 8.04				
12	Jan. 29, 1963	0508	13-38-47	136.8°E, 40.5°S	"	-2.39	- 6.97	.63	2.0	- 4.58	- 6.34	- 4.97				
13	Nov. 22, 1963	1431	18-34-39	171.1°W, 56.0°N	North Pacific Ocean	-0.08	- 3.46	3.44	3.4	- 3.38	- .02	- .06				
14		1435	18-38-16	170.4°W, 54.1°N	"	-0.08	- 6.52	3.44	3.4	- 6.44	- 3.08	- 3.12				
15		1437	18-40-01	170.0°W, 53.1°N	"	0.02	- 5.06	3.54	3.4	- 5.08	- 1.52	- 1.66				
16		1438	18-41-44	169.6°W, 52.1°N	"	0.16	- 5.59	3.54	3.4	- 5.75	- 2.05	- 2.19				
17		1440	18-43-24	169.3°W, 51.2°N	"	-0.90	- 6.66	3.32	3.2	- 5.76	- 3.34	- 3.46	0.614	-2.12	0.284 to 1.33	- 5.47 to 1.23
18		1442	18-45-02	169.0°W, 50.2°N	"	-0.44	- 5.53	3.42	3.2	- 5.09	- 2.11	- 2.33				
19		1445	18-48-09	168.4°W, 48.2°N	"	0.04	- 3.86	3.64	3.0	- 3.90	- .22	- .86				
20		1448	18-51-08	167.8°W, 46.3°N	"	-0.97	- 3.99	3.64	3.0	- 3.02	- .35	- .99				
21	Nov. 23, 1963	1428	18-35-11	155.1°W, 53.6°N	"	0.07	- 3.62	3.22	3.4	- 3.69	- .40	- .22				
22		1437	18-43-54	153.3°W, 48.8°N	"	0.03	- 4.65	3.32	3.4	- 4.68	- 1.33	- 1.25				
23		1438	18-45-24	153.0°W, 47.7°N	"	-1.16	- 3.90	3.42	3.2	- 2.74	- .48	- .70				
24		1440	18-46-50	152.7°W, 46.8°N	"	-0.76	- 3.47	3.42	3.2	- 2.71	- .05	- .27				
25		1441	18-48-11	152.5°W, 45.8°N	"	-0.50	- 3.54	3.42	3.2	- 3.04	- .12	- .34				

E. Double Ground Bounce Experiment

In an attempt to obtain a "bench mark" for comparison with the Alouette data an experiment has been designed to obtain variations in the ground reflection coefficient at a fixed location. This experiment will give useful information regarding the effect of ground moisture, snow, vegetation, etc., on the ground reflection coefficient.

Half-wave horizontal crossed-dipole antennas have been constructed. These antennas are placed a quarter wavelength about the ground. A 5.3 MHz carrier modulated by a 100μsec pulse at a rate of 100 pulses per second is directed vertically to the ionosphere. The first echo returns directly from the ionosphere. The second echo returns by way of the ionosphere, the ground, and the ionosphere. Therefore this is equivalent to a satellite transmitter at the image in the ionosphere.

If P_{R_1} is the power received on the first return then

$$P_{R_1} = \frac{W_T G k_I^2}{4\pi (2h)^2} \tag{8}$$

where $W_T G$ is the power radiated vertically by the antenna system, k_I is the ionosphere reflection coefficient and h is the height of the ionosphere. The power received on the second echo is

$$P_{R_2} = P_{R_1} \left(\frac{2h}{4h}\right)^2 k_g^2 k_I^2 \tag{9}$$

where k_g is the ground reflection coefficient. Thus,
In order to obtain k_g, we must first determine k_I from (8). The power radiated vertically from the antenna system, $W_T G$, must be determined also. This will be done by calculation and measurement. $W_T G$ will be kept constant for all data by adjusting the transmitter output.

To date the experiment is not yet operational.

V. DISCUSSION OF RESULTS

A. The velocity of the satellite, as specified on the date of September 29, 1962, at perigee was 16,467 miles per hour, and that at apogee was 16,387 miles per hour; it was at a height of 618.7 statute miles (995.7km) at perigee and 641.1 statute miles (1031.75 km) at apogee. During 7 milliseconds, roughly the time required for a radar pulse to travel twice the distance between the satellite and the earth (about 2,000 km) the satellite advanced only about 50 meters, or it turned an angle 4×10^{-4} degree around the center of the earth. With such a small movement, the satellite can be considered as stationary with respect to each individual radar pulse. Therefore, for each pulse the antenna pattern is considered a constant, even with the much slower satellite spin effect superimposed.

B. With the 100μ sec pulse and the 1000 km orbit, the first pulse length over the ground illuminates a circle with radius 173 km, corresponding to an illuminated cone with an apex angle of 20°. Because of this large angle and the relatively weak signals, the shape of the received pulse gives little information about the variation of scattering as a function of angle.

C. The dipole antenna on the satellite has a broad pattern and the satellite axis is inclined with respect to the radial direction by a maximum of around 20°. Consequently, no significant correction in the returns is required because of antenna tilt. It is assumed that the antenna pattern is the same as it would be if the antenna were in space. The antenna gain pattern is based on the calculated values supplied by the designer, the Sinclair Radio Laboratories.

D. No in-flight calibration of the satellite receiver system gain were possible. A series of calibrations, however, was carried out previous to launch. Errors may be introduced because the receiver sensitivity varies greatly for such small changes in the AGC level, and its measurement is not as precise as would be desirable.

E. The quiet day curve correction factors obtained range from .65 dB to 6.5 dB. It is evident that some of the large correction factors are not quite reliable because they result in $K_g > 1$ (line 2,3; Column B, Table 5). This may be contributed to the fact that some of the assumptions for using the quiet day curve are perhaps not fully justified. These assumptions are listed in paragraph B, Section IV.

G. The average diurnal attenuation correction factors ranged from .5 to 3.5 dB. They were obtained from figure 3 (summer: May through October inclusive) and figure 4 (winter: November through April inclusive). These corrections give quite consistent results. That is, there are no obviously wrong corrections as in Column B, Table 5, lines 2 and 3 which indicate $K_g > 1$.

Similarly, in Column A, Table 5 lines 2, 5, 10, 15, 16, 19, 21 and 22 indicate the correction was made using $K_i > 1$.

The variation in K_g (Column C, Table 5) for the ocean (lines 1 through 5 inclusive) may be due to the sea state. Lines 6 through 10 inclusive are returns from the Australian Continent and are certainly consistent in that it is expected that K_g for land is less than K_g for salt water. Similarly for (line 12) the forested area in Australia. At this frequency a forest can be expected to introduce considerable scatter.

Lines 13 through 25 inclusive are points obtained over the North Pacific and again are consistent with theory.

Table 5 also lists the averages for the various areas and the ranges of the results using the $\pm$ 3.35 dB overall RMS error expected.

VI. CONCLUSIONS

The observation of effective reflection coefficients from the 1000 km altitude of the Alouette satellite have been made for 70 sample points over the earth surface, at frequencies in the order of 9 Mc/s. The absolute calculated ground effective reflection coefficient ranges from -12 dB to -2.8 dB for land and 09.2 dB to -2.68 dB for the ocean. Estimated

variability of the data is ± 3.35 dB. By applying the first order correction from the quiet day curve, the ionosphere absorption ranges from 0.65 dB to 6.5 dB at 9 Mc/s and the corrected values range from -10.5 dB for the forest to -0.02 dB for the ocean. The average diurnal attenuation correction gives ranges of -5.35 dB to -0.06 dB for the ocean and -10.67 dB to -4.6 dB for land.

VIII. APPENDIX

The relation between $\omega_N^2 = N_e^2/\epsilon_o m$ and $\omega_H = \mu_o H_o e/m$

where N = the electron density of the ionosphere

H_o= the total earth magnetic field without concerning with the location in the space,

can be estimated by assuming

1. For the vertical incident case the horizontal deviation of the ordinary and the extraordinary wave from the vertical plane of incidence may be ignored.

2. The strength of the earth's magnetic field decreases monotonically as the point of reflection getting deeper into the space.

3. The collision in the ionosphere along the wave traveling path is negligibly small.

4. It is the same layer that reflects the ordinary and the extraordinary wave at the electron density maximum, as well as at the Alouette satellite level. Therefore, at these two particular points of reflection, the signal frequencies for the ordinary and the extraordinary wave are related through the equations

$$\omega_N = \omega_o = \omega_E \left(1 - \frac{\omega_H}{\omega_E}\right)$$

5. The relation between the ordinary and the extraordinary wave frequencies is assumed to be fit by the polynomial

$$\omega_o = \sum_{i=u}^{n} a_i (\omega_E)^i$$

After working over several examples it is found that the simplest fit

$$\omega_o = a_o + a_1 \omega_E$$

is the best approximation. For any given ω_o the ordinary wave, the frequency ω_E of the extraordinary wave corresponding to the same reflecting layer may thus be determined, and the gyro-frequency, ω_H accordingly the geomagnetic field strength, H, at this layer can be calculated from the relation

$$\omega_H = (1 - \frac{\omega_o}{\omega_E})\omega_E$$

$$H = \frac{m\omega_H}{\mu_o e}$$

Note that these results will have nothing to do with altitude. The electron density profile must be solved by employing methods suggested, for example, by Titheridge [1961], Unz [1964], etc.

In case the absorption in the ionosphere cannot be ignored completely, the wave reflection index μ will no longer be reduced to zero when reflection occurs. As long as the collision frequency ν is small comparing with the signal frequency ω, the relations engaged in the discussion are held true approximately [Ratcliffe, 1959]. Relations among ω_o, ω_E, and ω_H should still be valid within acceptable error limits.

Alouette Calibration Curves

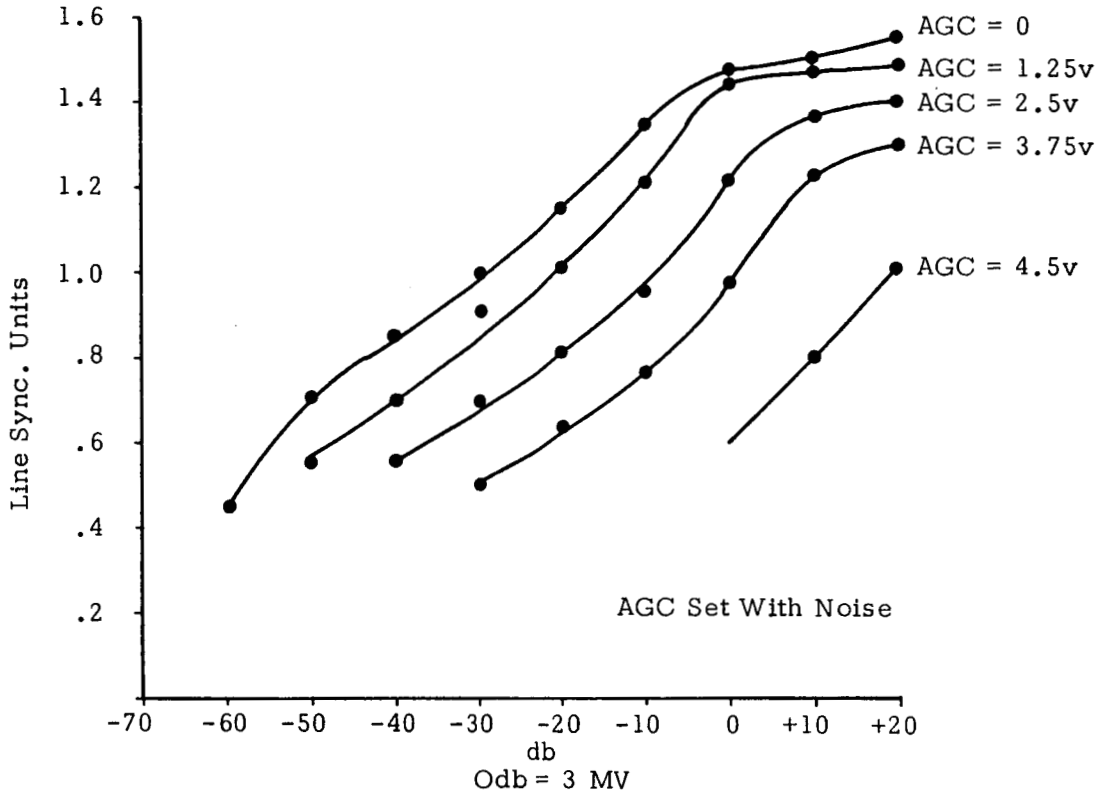

S-27-6 RX 3 MHz

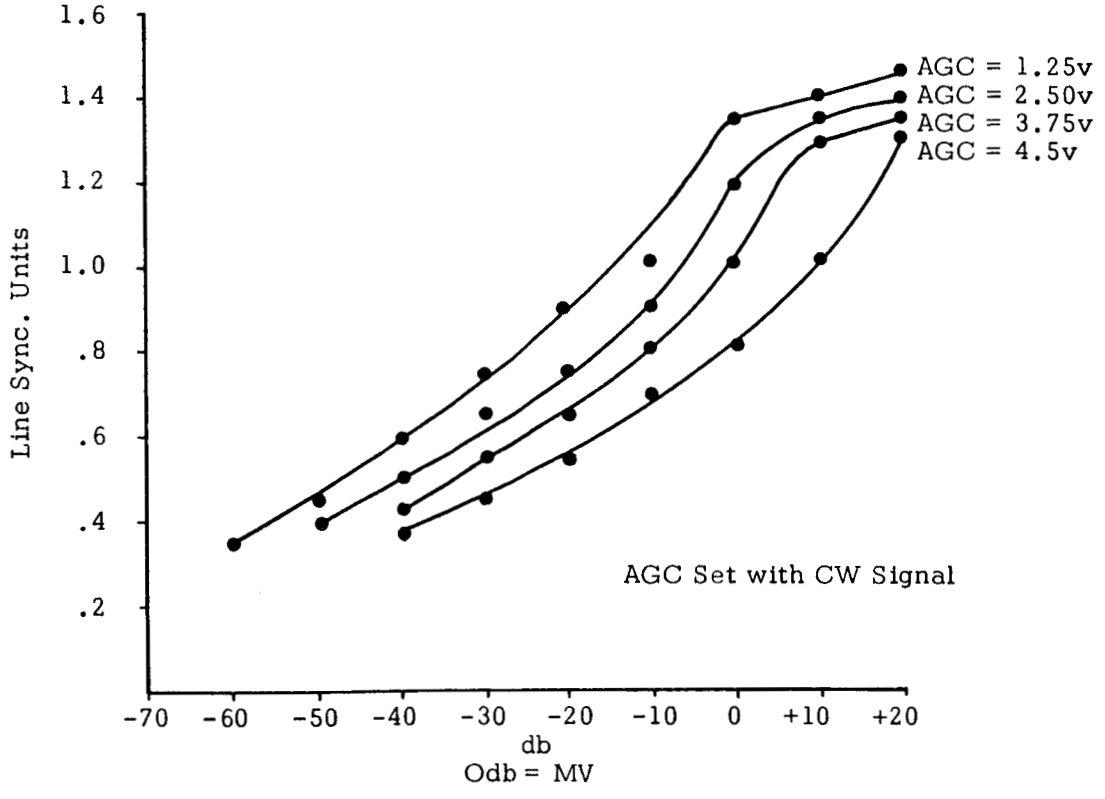

Figure 5.

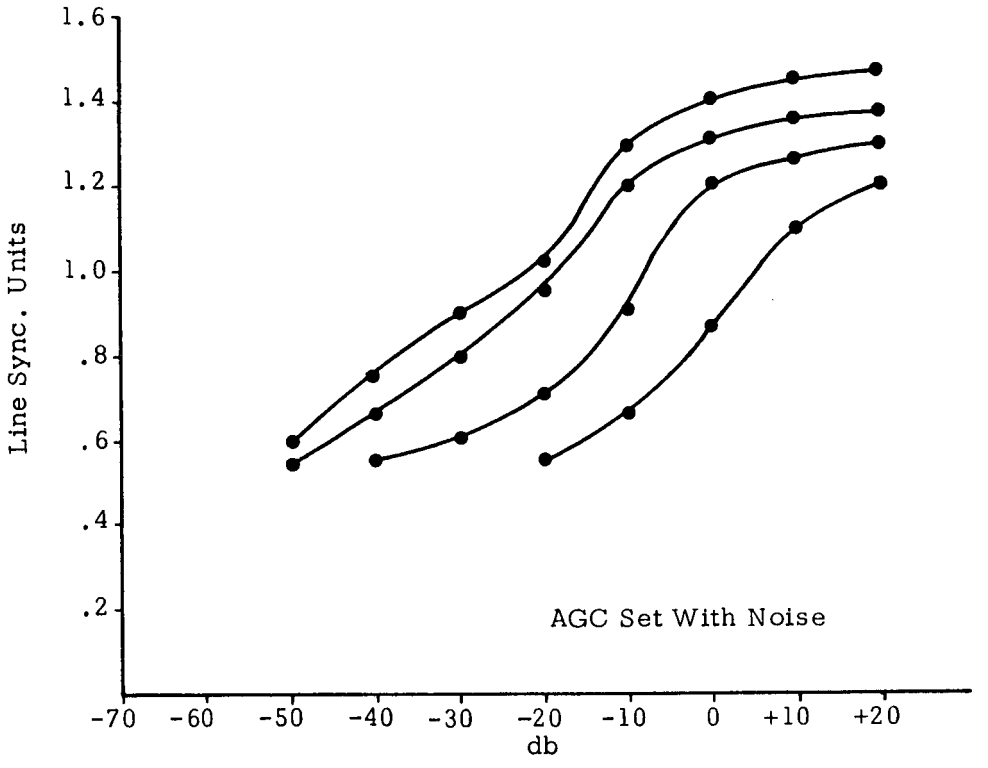

Odb = 3 MV

S-27-6 RX 9 MHz

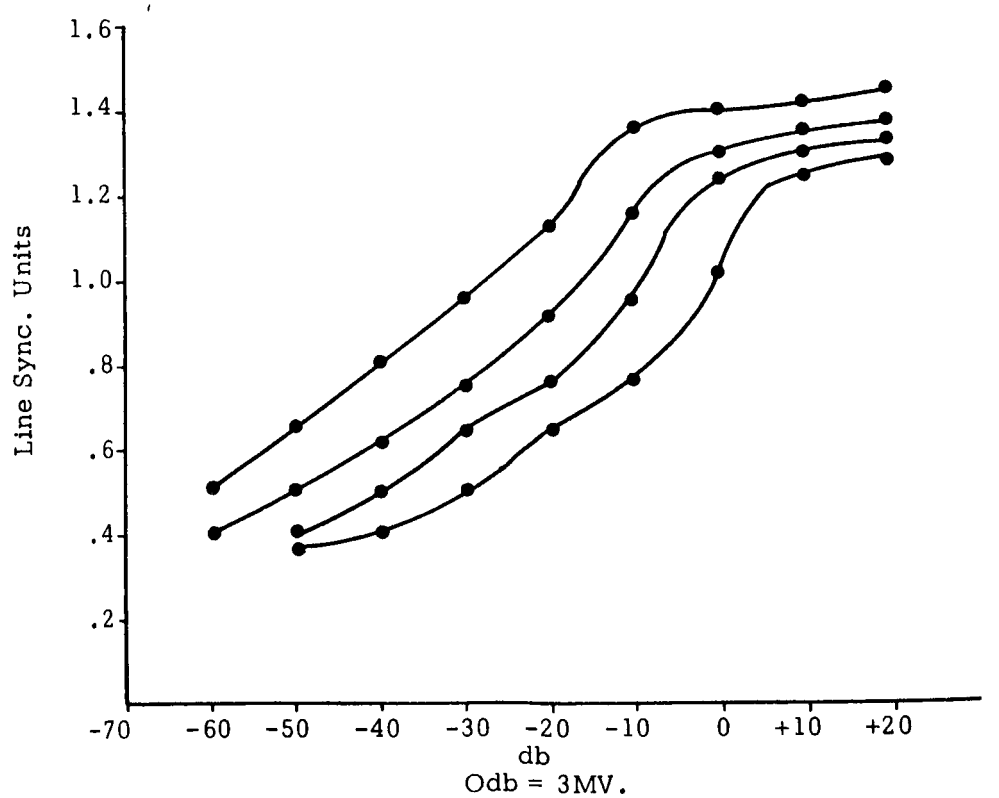

Odb = 3MV.

Figure 6.

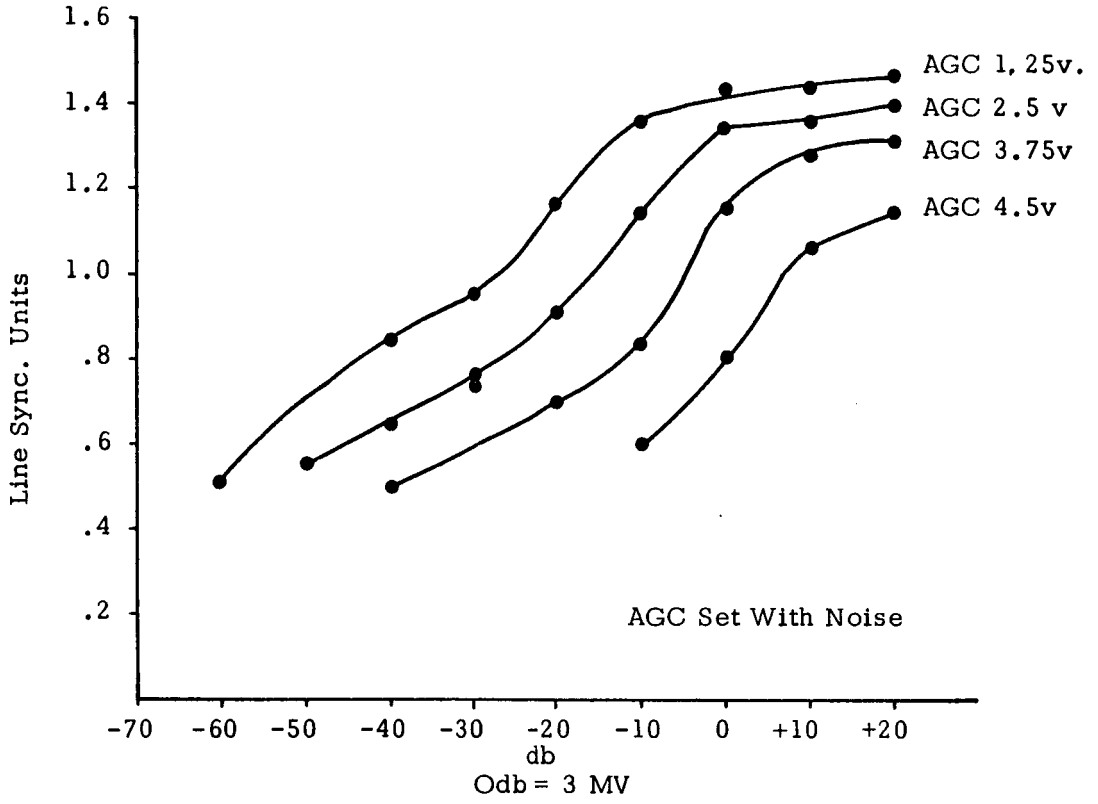

S-27-6 RX 6MHz

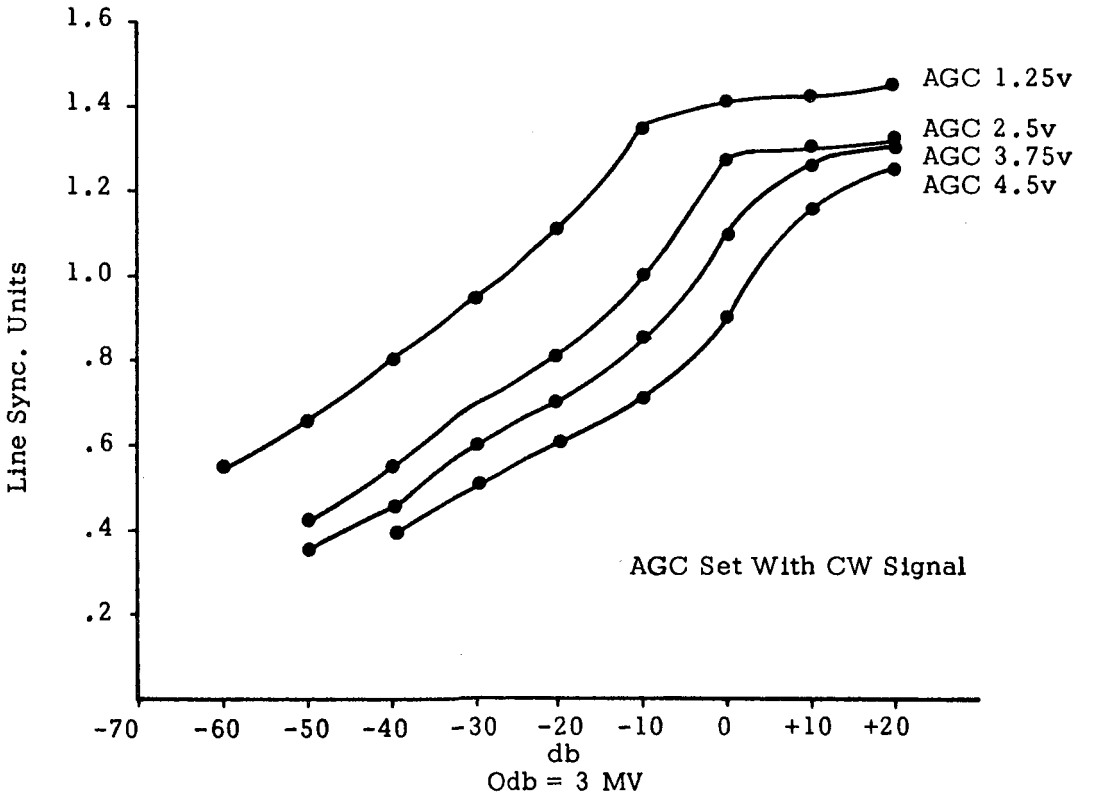

Figure 7.

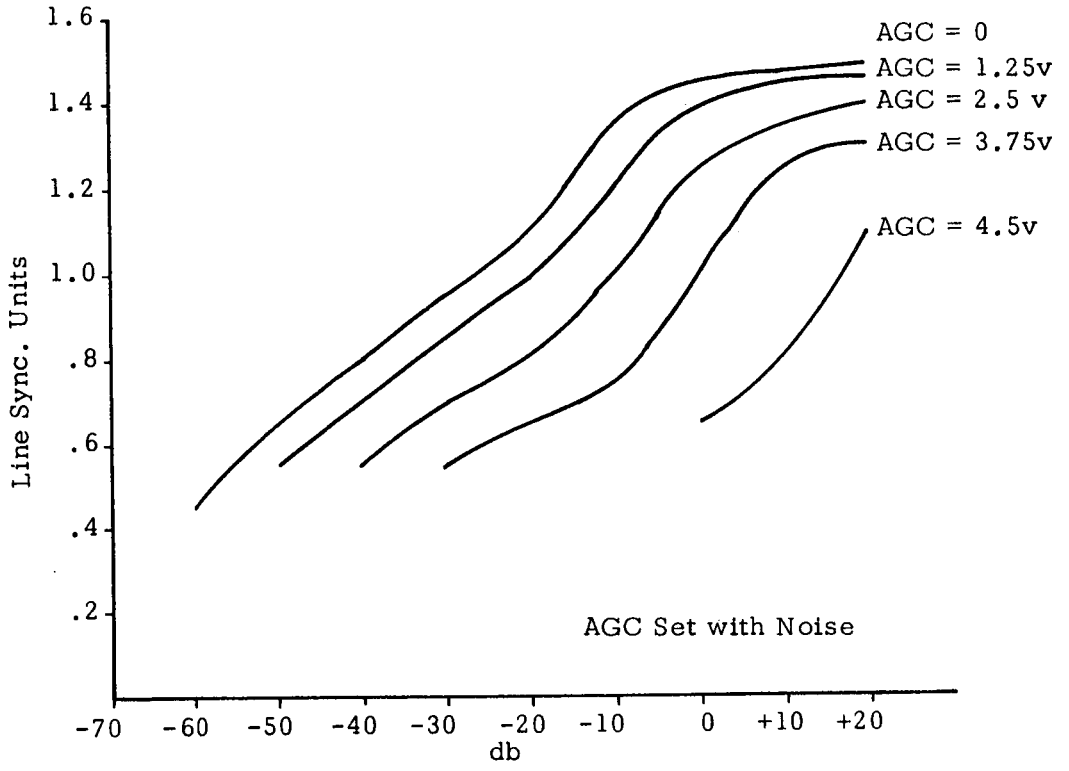

Odb = 3 MV.

S-27-6 RX 12 MHz

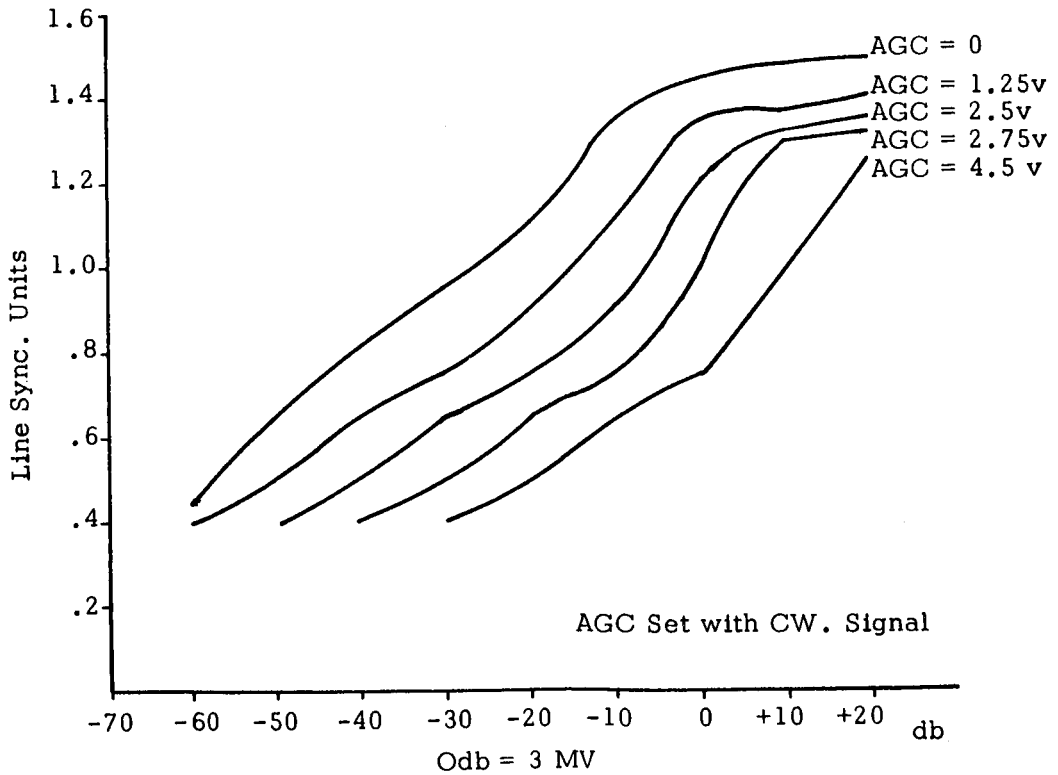

Odb = 3 MV

Figure 8.

SIGNAL AT RECEIVER INPUT

Supply Voltage 15.4 v

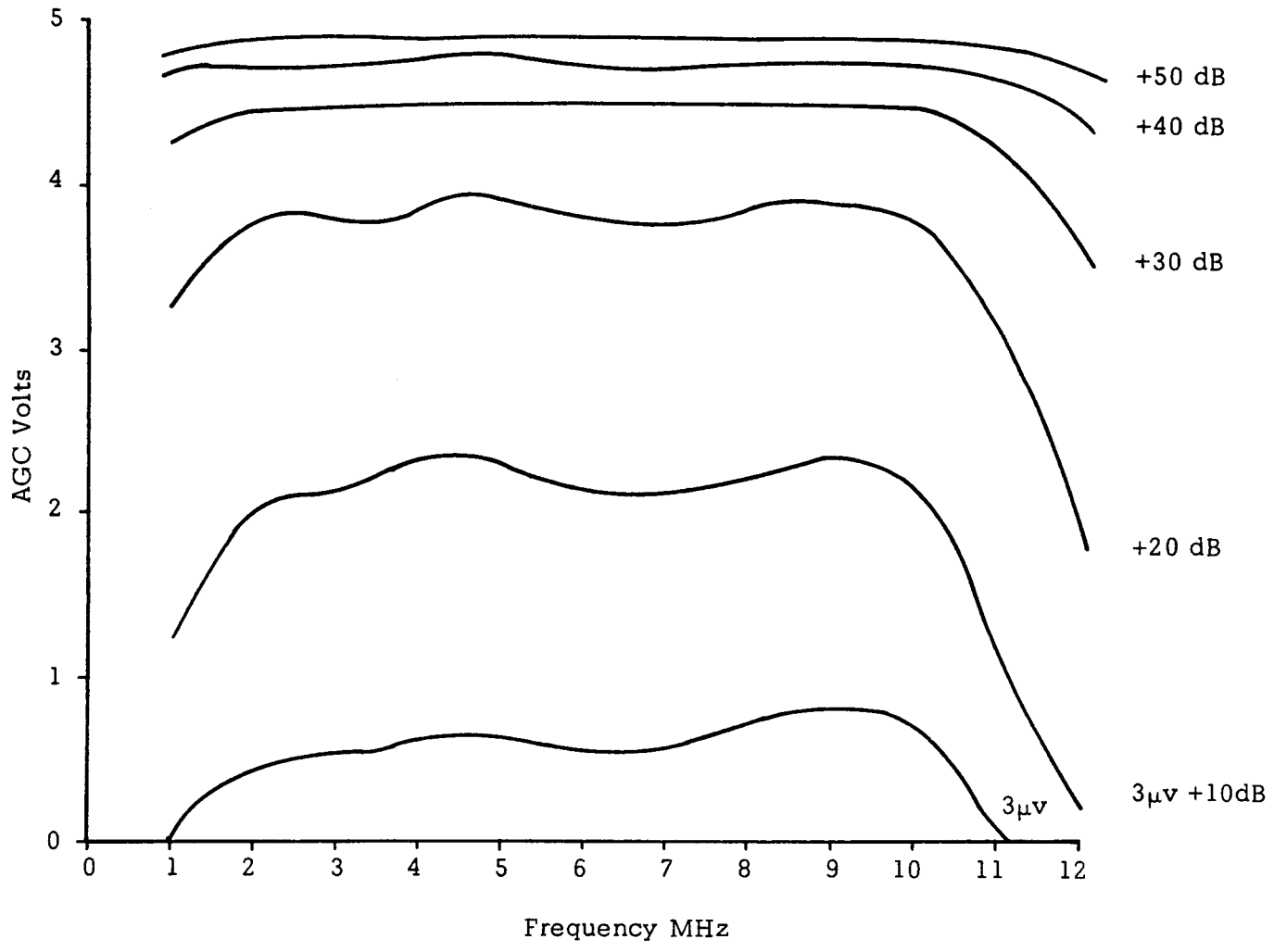

Figure 9.

CALCULATED CURVES

RADIATED POWER w.r.t. OPTIMUM

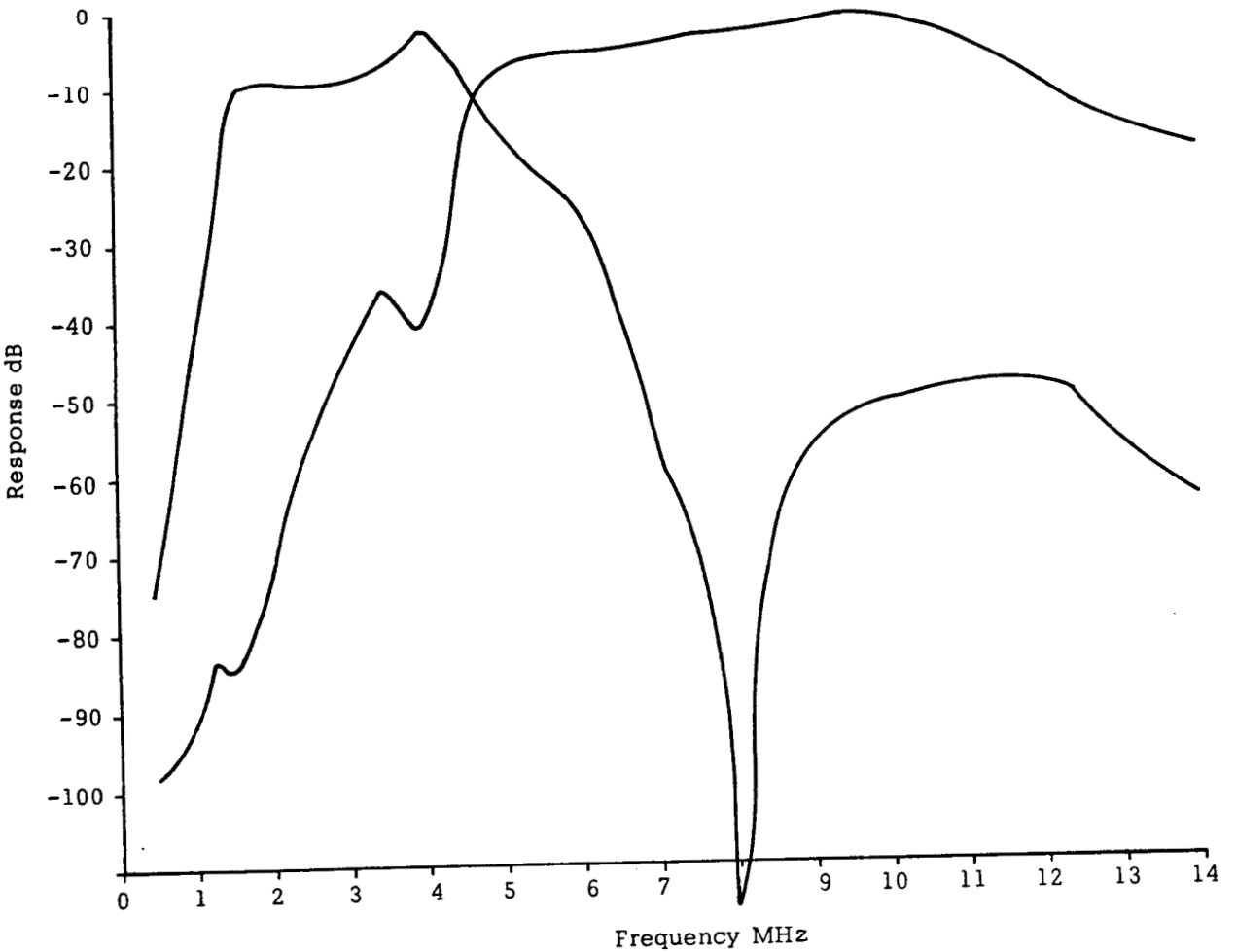

Figure 10.

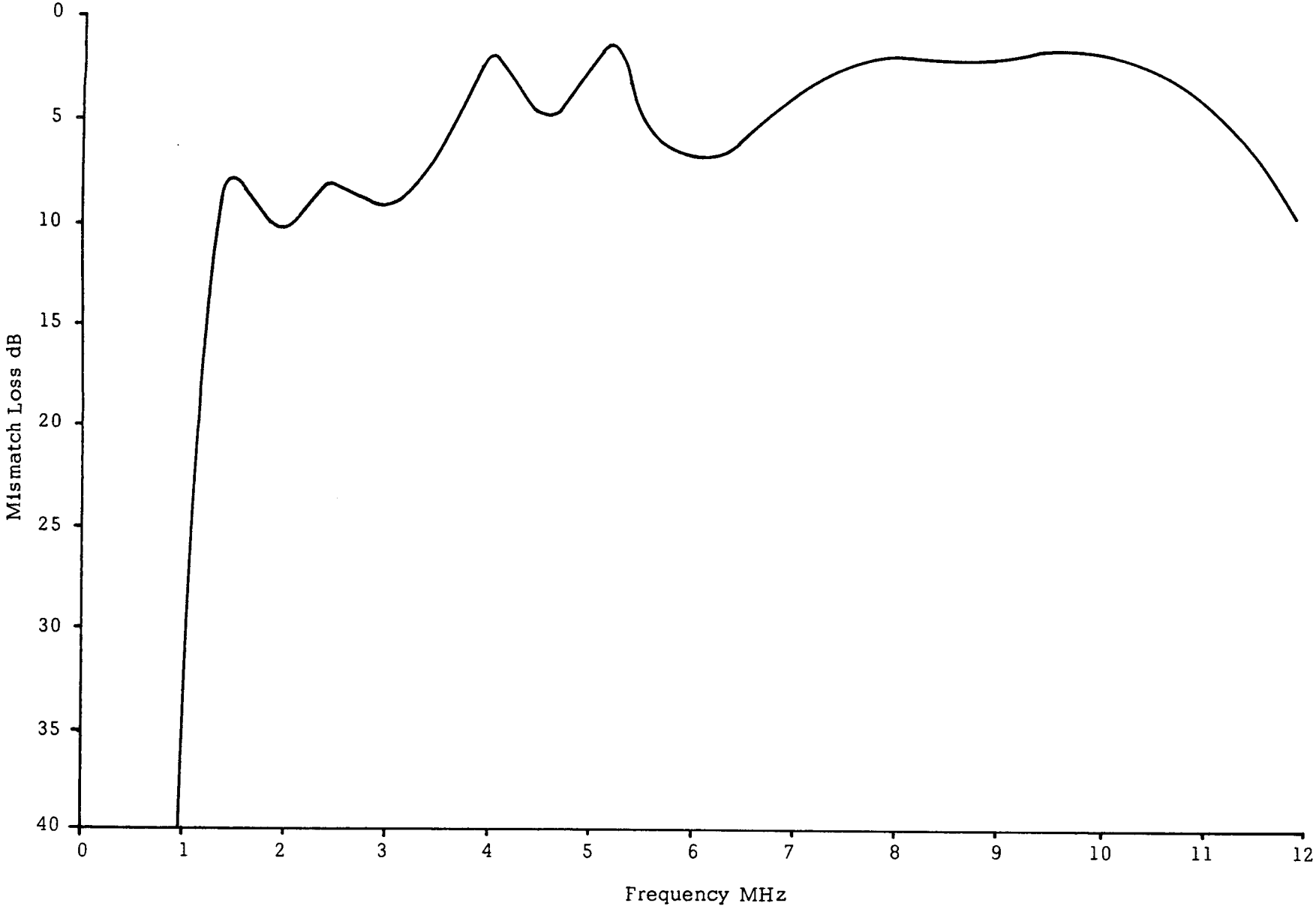
0
5
10
15
20
25
30
35
40
Mismatch Loss dB
0
1
2
3
4
5
6
7
8
9
10
11
12
Frequency MHz

Figure 11.

S-27-4 TRANSMITTER OUTPUT

INTO SIMULATED ANTENNA IMPEDANCES

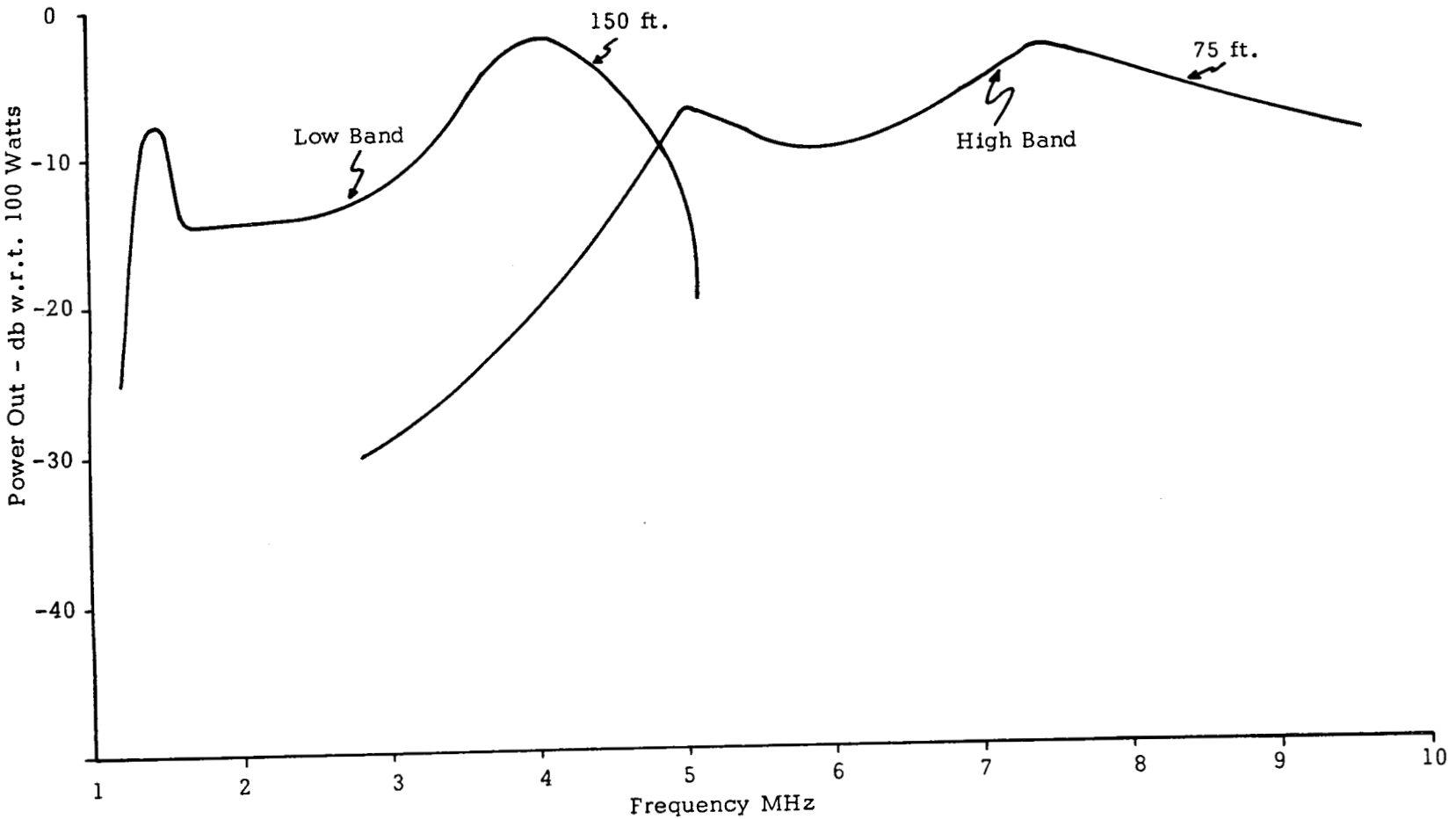

Figure 12.

AGC VARIATION WITH SUPPLY VOLTAGE

10 μv at 4 MHz Input

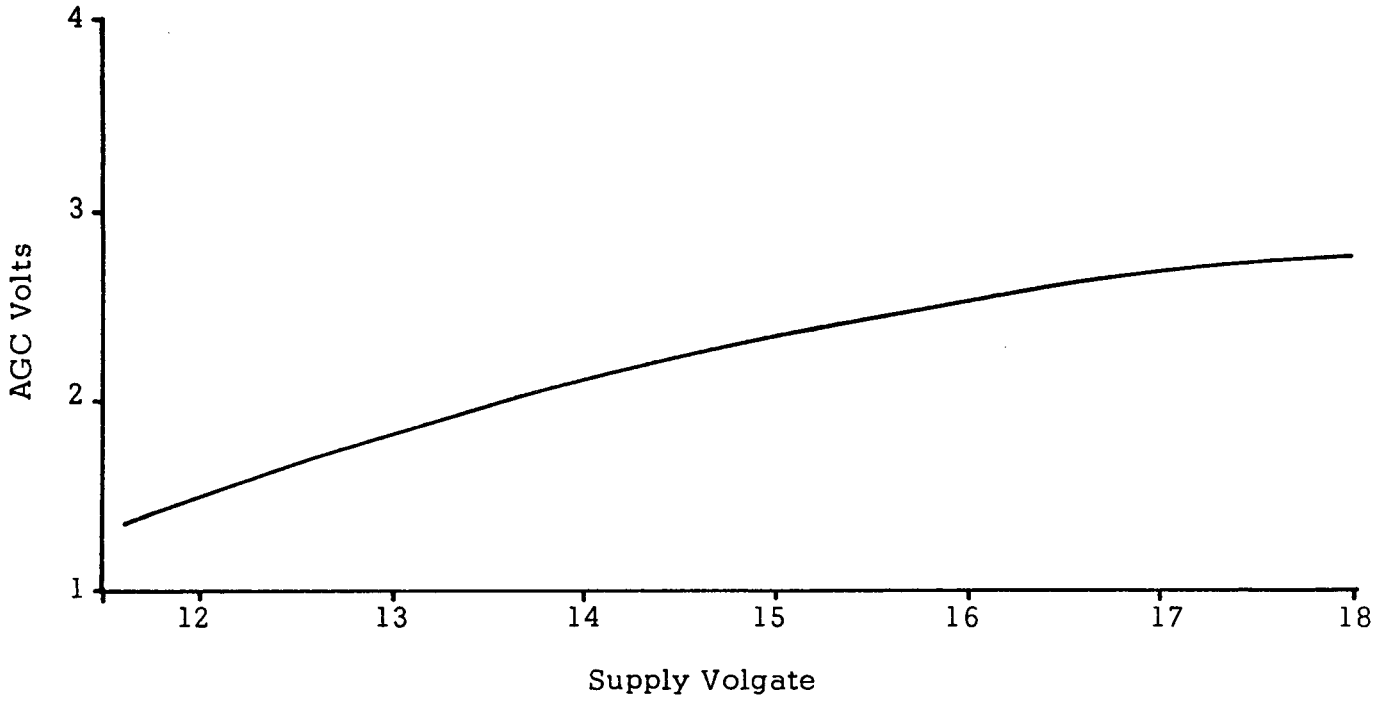

Figure 13.

References

Chia, R. C., A. K. Fung and R. K. Moore, "High Frequency Backscatter from the Earth Measured at 1000 Km Altitude," Radio Science, Journal of Research NBS/USNC-URSI, vol. 69D, no. 4, April 1965, pp. 641-649.

Edison, A. R., R. K. Moore and B. D. Warner, "Radar Terrain Return Measured at Near-Vertical Incidence," IRE Trans. Ant. Prop., vol. 8, no. 3, May 1960, pp. 246-254.

Hayre, H. S., "Radar Backscatter Theories for Near-Vertical Incidence and Their Application to an Estimate of the Lunar Surface Roughness, University of New Mexico, Doctoral dissertation, 1962.

Mitra, A. P. and C. A. Shain, "The Measurement of Ionospheric Absorption Using Observations of 18.3 Mc/s Cosmic Radio Noise," J. Atmos. Terr. Phys., vol. 4, 1953, pp. 204-218.

Moore, R. K., "Resolution of Vertical Incidence Radar Return into Specular Components," University of New Mexico, Engr. Expt. Sta. Tech. Rept. EE-6, July 1957.

Ratcliffe, J. A., Magneto-Ionic Theory, Cambridge University Press, 1959.

Taylor, R. C., "Terrain Return Measurement at X, K_u, and K_a Band, IRE Nat. Conv. Record, vol. 7, part 1, 1959, pp. 19-26.

Titheridge, J. E., "A New Method for the Analysis of h'(f) Record," J. Atmos. Terr. Phys., vol. 21, no. 1, April 1961.

Unz, H., "The Reduction of Ionograms to Electron Density Profile," J. Atmos. Terr. Phys., vol. 26, no. 1, Jan. 1964.

CRES LABORATORIES

Chemical Engineering Low Temperature Laboratory

Remote Sensing Laboratory

Electronics Research Laboratory

Chemical Engineering Heat Transfer Laboratory

Nuclear Engineering Laboratory

Environmental Health Engineering Laboratory

Digital Computer Technology Laboratory

Water Resources Institute

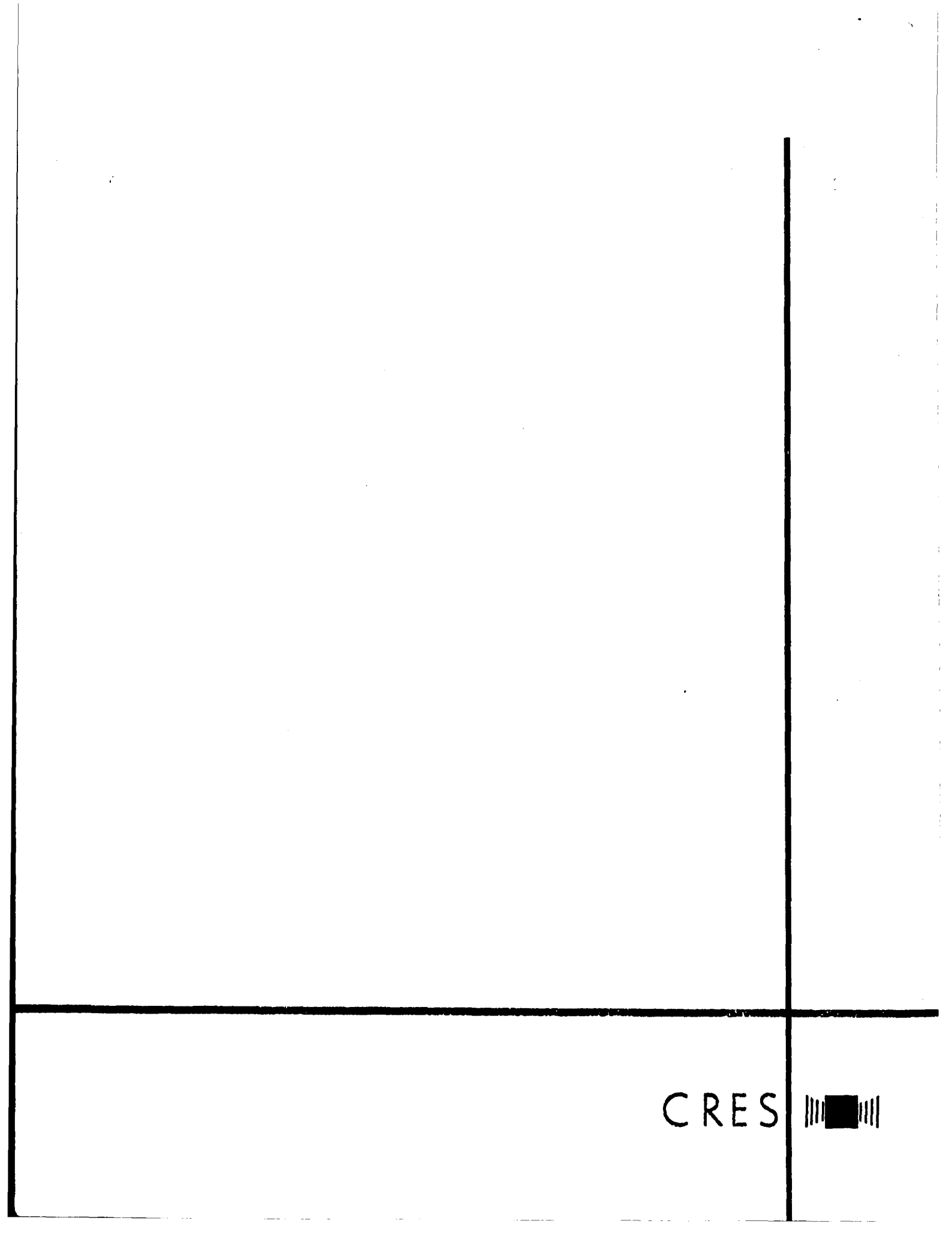
CRES